Available Online at http://www.jart.ma

Journal of Atlantic Research and Technology

Efficient Adsorption of Methylene Blue onto Pyrophyllite Clay: A Low-Cost Wastewater Remediation Strategy

Charifa Agdid[a], Mahir Fatima-Zahra[a], Mohamed Rhaya[a], Brahim Ennasraoui[a], Youssef Miyah[b,c], Hassan Ouachtak[a,d], Rachid El Haouti[a,d], Ali Laghzal[a,e], Said Alahiane[a,d], Abdelaziz Ait Addi[a]

[a] *Laboratory of Organic and Physical Chemistry, Faculty of Science, Ibn Zohr University, Agadir, Morocco*
[b] *Laboratory of Materials, Processes, Catalysis, and Environment, Higher School of technology, University Sidi Mohamed Ben Abdellah, Fez, Morocco*
[c] *Ministry of Health and Social Protection, Higher Institute of Nursing Professions and Health Techniques, Fez, Morocco*
[d] *Faculty of Applied Science, Ait Melloul, Ibn Zohr University, Agadir, Morocco*
[e] *High Institute of Marine Fisheries (ISPM), Fisheries Department, 80000 Agadir, Morocco*

ARTICLE INFO

Article history:
Received 25th September, 2025
Received in revised form 15th November, 2025
Accepted 19th November, 2025
Available online 31th December, 2025

Keywords:
Anionic surfactants
Methylene Blue Active Substances
Spectrophotometry
Water Analysis
Liquid-Liquid Extraction

ABSTRACT

This study evaluates pyrophyllite clay as an efficient adsorbent for methylene blue (MB) removal from aqueous solutions. The clay was characterized via XRD, SEM-EDX, and FTIR to elucidate its structural, morphological, and functional properties. Batch adsorption experiments systematically examined the effects of adsorbent dosage, contact time, solution pH, and initial MB concentration, revealing optimal performance with pH-dependent uptake peaking in both acidic and basic ranges. Langmuir isotherm analysis determined a maximum adsorption capacity (q_{max}) of 69.44 mg/g, indicative of monolayer coverage. Kinetic data best fitted the pseudo-second-order model ($R^2 > 0.99$), confirming chemisorption as the rate-limiting step. Thermodynamic parameters ($\Delta G° < 0$, $\Delta H° > 0$) and negative interaction energies from molecular simulations further demonstrated spontaneous, endothermic, and thermodynamically favorable adsorption processes, aligning closely with experimental findings. These results highlight pyrophyllite's potential as a low-cost, eco-friendly alternative for dye-laden wastewater remediation.

1. Introduction

The presence of chemical dyes, especially methylene blue (MB, $C_{16}H_{18}ClN_3S$), is one of the major reasons of water pollution and, as a result, they are considered to be the most serious threat to fish life and humans because they are not easily degradable, and are generally very toxic, and ability to accumulate in tissues [1]. The world market for MB is more than 700,000 tons each year and even such a small quantity as 1-10 mg/L cause bleaching of the light-dependent plant stage and bio-mutation of the organisms [2]. Common methods of dye treatment like coagulation and advanced oxidation processes are expensive, create sludge, and therefore, it is necessary to find cheaper and more environmentally-friendly options, like natural clay-based adsorbents [3,4]. Pyrophyllite ($Al_2Si_4O_{10}(OH)_2$) is one of the few 1:1 layered aluminosilicates with a composition predominantly of silica (~55% SiO_2), thus it possesses low cation exchange capacity and moderate surface area [5,6]. Due to these very properties, it can be used for the effective uptake of cationic dyes such as MB through ion exchange and surface complexation methods. Its acid activation increases the veracity of its pores and its adsorption capacity [7], while the Moroccan variants of pyrophyllite, containing quartz, illite, smectite, and kaolinite, obtain negatively charged surfaces at the pH > pH_{pzc} for dye binding to be most productive [8,9]. The process of MB adsorption takes place through electrostatic attraction at neutral-alkaline pH (7-12), plus it is supported by means of hydrogen bonding and π-π interactions

* Abdelaziz Ait Addi.

E-mail address

[10,11]. The most recent developments are basically the use of pyrophyllite-derived geopolymers that are porous for the enhanced removal of dyes, the production of clays with thermal stability that have more than 85% regeneration over five cycles through adsorption-thermolysis, and the acid-activated [12]. Moroccan clays that are giving more than 90% MB removal at very low dosages (0.5 - 2 g/L) [13]. But even with the above progress, problems regarding industrial scale-up and the control of secondary pollution still exist, thus making it very necessary to carry out intensive research on kinetics, isotherms, and reusability studies to come up with methods that are in line with the sustainable water goals [14]. This study investigates MB adsorption onto raw and activated pyrophyllite from aqueous solutions, evaluating key parameters including contact time, solution pH, and initial dye concentration. Adsorption kinetics were modelled using pseudo-first-order and pseudo-second-order equations to determine rate constants, while equilibrium data were fitted to Langmuir and Freundlich isotherms to assess maximum capacity and adsorption affinity.

2. Materials and Methods

2.1. Chemicals

The commercial cationic textile dye methylene blue (MB), used in this study, was purchased from Sigma-Aldrich and employed without further purification. Its characteristics are summarized in Table 1. Aqueous MB solutions were prepared by dissolving the required dye mass in bidistilled water [15,16].

Table 1.
Characteristics of Methylene Blue.

Name	**Methylene blue**
Chemical structure	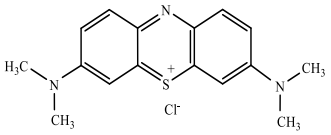
Family	Thiazine
Molecular formula	$C_{16}H_{18}ClN_3S$
IUPAC name	3,7-Bis(dimethylamino)phenazathionium chloride
Molar mass (g/mol)	319,85
Solubility in water (g/L) at 20 °C	40
Melting point (°C)	190
λ_{max}(nm)	664

2.2. Chemical composition of the adsorbent

Pyrophyllite, an aluminosilicate clay with the chemical formula $Al_2Si_4O_{10}(OH)_2$, is a dioctahedral 2:1 (TOT) layered mineral consisting of one octahedral sheet sandwiched between two tetrahedral sheets [17]. All tetrahedral sites are occupied by Si^{4+} ions, while two-thirds of the octahedral sites contain Al^{3+} ions, leaving the remaining third vacant. The electrically neutral TOT layers are held together by weak van der Waals forces [18].

2.3. PZC determination

The point of zero charge (pH_{PZC}) for pyrophyllite samples was determined using a standard batch equilibration method. Nine vials, each containing 0.05 g of adsorbent in solutions adjusted to initial pH values (pH_i) from 2 to 10, were stirred for 24 h at room temperature. After filtration, the final pH (pH_f) of the supernatants was measured using a pH meter with a glass electrode. The difference ($\Delta pH = pH_f - pH_i$) was plotted against pH_i, with the intersection at $\Delta pH=0$ defining the pH_{PZC}, which indicates the net surface charge neutrality of the adsorbent [19].

2.4. Characterization methods

FTIR spectra of pristine pyrophyllite and dye-loaded pyrophyllite were recorded using a Shimadzu spectrometer fitted with a Jasco ATR PRO ONE module (resolution: 16 cm^{-1}) at room temperature over 4000–400 cm^{-1}. For transmission measurements, samples before and after dye adsorption were homogenized with KBr. XRD patterns of pyrophyllite were obtained via diffractometer Bruker D8 ADVANCE TWIN model in transmission mode, operating at 40 kV and 40 mA, scanning 5°–80° 2θ (step size: 0.02°, rate: 0.3 s/step) with Cu Kα radiation (λ = 1.5418 Å). Surface morphology was examined by SEM called JEOL JSM-IT100LA at up to 20 kV, coupled with EDX for elemental analysis [20].

2.5. Adsorption experiments

To study the effect of each parameter on the adsorption of MB onto the adsorbent, a specific approach was followed in this study. The experiments were conducted using the static method with different initial adsorbent masses and pollutant concentrations. The adsorption tests involved adding a precise amount of adsorbent to 20 ml of adsorbate solution in a 100 ml beaker under constant magnetic stirring and at a constant temperature of 25 °C. After 120 minutes of stirring, the samples were separated from the adsorbent using a Millipore filter with a porosity of 0.45 µm. The filtrates were then analysed by UV/Visible spectrophotometry at the wavelength corresponding to the maximum absorbance of the MB solution (λ = 664 nm). Adsorption experiments were carried out by modifying the pH of the initial solution, the contact time, the adsorbent dose, the initial MB concentration and the temperature for the adsorption kinetics, adsorption isotherm and thermodynamic study.

The amount of methylene blue dye adsorbed by pyrophyllite clay was calculated using equation 1 [21]:

$$Q_t = \frac{(C_0 - C_e)V}{m} \qquad \text{(Eq.1)}$$

where C_0 (mg/L) and C_t (mg/L) are respectively the initial concentration and the concentration at time t or the equilibrium concentration of the dye; m (g) is the mass of adsorbent used, and V (L) is the volume of the solution.

The percentage removal of dyes (R %) was expressed as follows [22]:

$$R(\%) = \frac{C_0 - C_e}{C_0} \times 100 \qquad \text{(Eq.2)}$$

3. Results and discussion

3.1. Characterization of pyrophyllite

3.1.1. XRD analysis

Figure 1 shows the diffractogram obtained for the mineralogical analysis of the sample, revealing the predominant presence of two crystalline phases: pyrophyllite and quartz. As illustrated in Figure 1, several diffraction peaks appear at the following 2θ angles: 9.167° (002), 4.590° (004), 3.341° (113), 3.062° (006), 2.425° (1.368) and 117° (316), which correspond to the characteristic crystallographic planes of pyrophyllite. Moreover, the peaks located at 3.343° (101) and 1.817° (112) are associated with the presence of quartz [23]. These results are consistent with those reported in the literature, where several studies have identified the same peak positions for pyrophyllite, thus confirming the validity of our analysis and the correct identification of the mineral phases present in the sample [24].

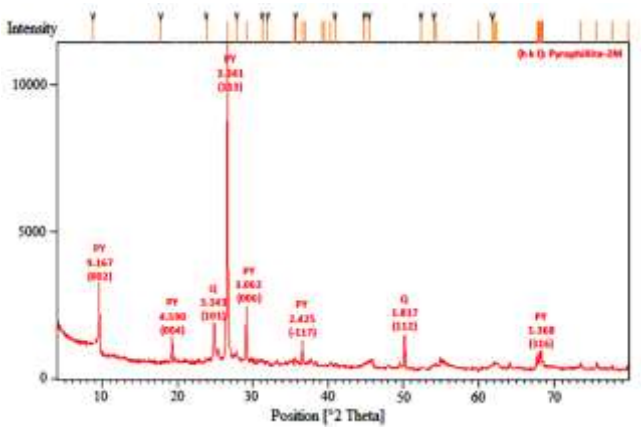

Fig.1. XRD pattern of pyrophyllite

3.1.2. SEM analysis

The pyrophyllite sample was analyzed using SEM combined with EDX in order to better characterize its morphological properties and elemental composition. Figure 2 presents the SEM micrographs obtained, along with the corresponding EDX spectrum, confirming the silicate nature of the pyrophyllite and highlighting the distribution of major elements such as silicon (Si), aluminium (Al), and oxygen (O). The SEM images reveal a heterogeneous morphology of the pyrophyllite and show a porous surface, which helps facilitate the adsorption of materials. In addition, the EDX spectrum shows the presence of the previously mentioned elements, namely Al, Si, Na, Mg, Fe, and Ca [25,26].

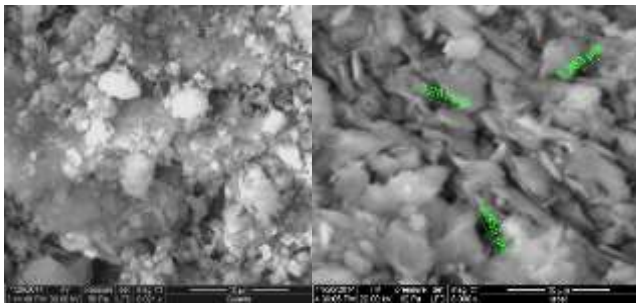

c)

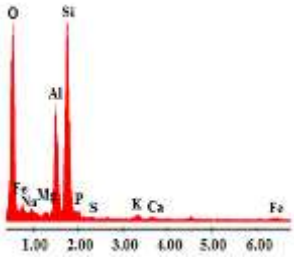

Element	% mass	% atomic
O	27.0	38.9
Na	4.9	4.9
Mg	3.0	2.8
Al	23.2	19.8
Si	36.8	30.3
P	1.7	1.3
S	0.7	0.5
K	1.4	0.8
Ca	0.6	0.3
Fe	0.8	0.3
Total	100.0	100.0

Fig. 2. Morphological Analysis of Pyrophyllite by SEM Coupled with EDX

3.1.3. FTIR analysis

Fourier Transform Infrared (FTIR) analysis was used to identify the characteristic functional groups present in the structure of the pyrophyllite. According to Figure 3, the obtained spectrum highlights absorption bands typical of pyrophyllite, notably those attributed to OH, Si–O, and Al–O bond vibrations [27].

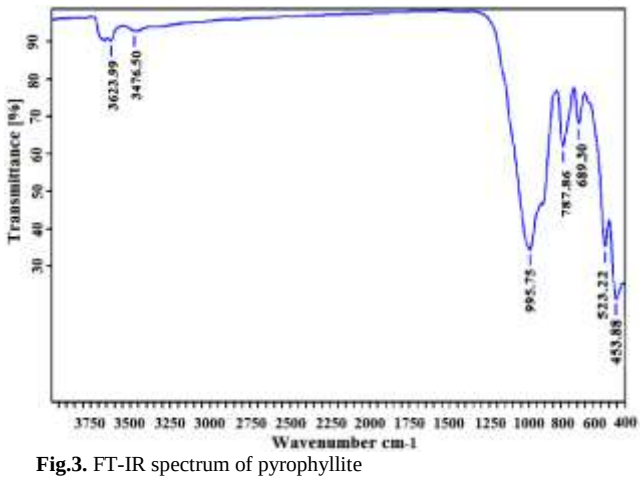

Fig.3. FT-IR spectrum of pyrophyllite

The results of this analysis confirm the presence of the characteristic groups of this phyllosilicate mineral. The bands located at 3623.99 and 3476.50 cm^{-1} correspond to

the stretching vibration of the OH group of structural water; the band at 995.75 cm^{-1} corresponds to the valence vibration of the Si–O bond, the band at 787.86 cm^{-1} corresponds to the O–Si–O bond, and the band at 689.30 cm^{-1} characterizes the Al–O and Si–O bonds [28]. The last two bands located at 523.22 and 453.88 cm^{-1} correspond to the deformation vibrations of O–Si–Al [27]. Overall, the observation of these spectrometric absorption bands confirms the presence of bonds specific to pyrophyllite [29].

3.2. Adsorption of MB dye on Pyrophyllite

3.2.1. pH effect

pH is an important factor in the adsorption process, as it affects both the surface of the adsorbent and the ionization state of the adsorbate, thereby influencing their interfacial interactions [30]. Figures 4 and 5 illustrate the results of a study on the influence of pH on the removal of MB over a pH range from 2 to 10. The initial concentration of the adsorbate was fixed at 20 ppm in a solution volume of 20 mL. The pH at the point of zero charge was measured at 6.56. This behavior may be attributed to the fact that the surface of pyrophyllite clay is positively charged when pH < pH_{PZC}, and negatively charged when pH > pH_{PZC}. The optimal adsorption pH was observed at pH = 6. Analysis of these results shows an increase in MB removal efficiency over the entire pH range studied, indicating that pH does not have a significant effect on adsorption.

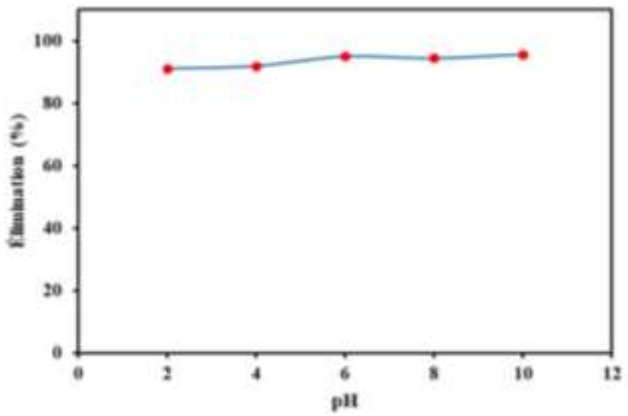

Fig.4. Influence of pH on the Adsorption Efficiency of MB Dye on pyrophyllite ($[MB]_0$=20 mg/L, t=80 min, R=0,5 g /L et T=25 °C)

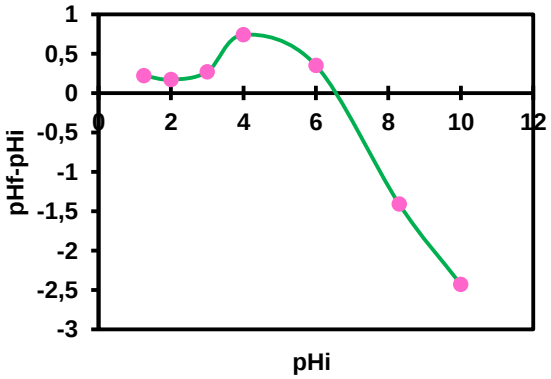

Fig.5. Typical Plots of pH_f-pH_i vs. pH_i for the estimation of pHpzc of pyrophyllite

3.2.2. Adsorbent mass effect

The adsorbent mass has two essential effects on the adsorption process. On one hand, its increase can lead to a larger solid/solute contact surface, and on the other hand, the number of active sites is proportional to the mass of the support [31]. To study the effect of adsorbent mass, the initial concentration of the adsorbate was fixed at 20 mg/L in a solution volume of 20 mL at the optimal pH of 6.84. Different adsorbent masses (2.5, 5, 10, 15, 20, 30, 40 mg) were used, with a contact time of 2 hours at 25°C. Adsorption relies on the transfer of matter from the liquid phase to the solid phase. Thus, the adsorbent mass significantly influences the efficiency of the adsorption process. The results obtained, illustrated in Figure 6, show that the adsorption efficiency increases with the adsorbent mass, reaching a maximum of 95.12 % MB removal when the adsorbent mass is 10 mg. Beyond this dose, the adsorption percentage remains nearly constant, indicating that equilibrium has been reached. This can be explained by the increase in the specific surface area of the adsorbent and the availability of additional adsorption sites until saturation [32].

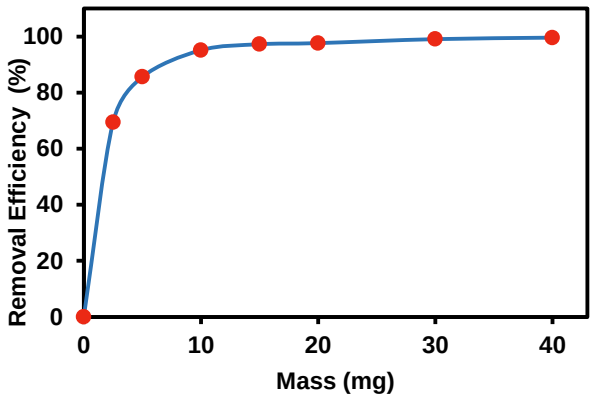

Fig.6. Effect of Adsorbent Mass on MB Removal Efficiency (pH = 6.84, $[MB]_0$=20 mg/L, t=120 min, T = 25 °C)

3.2.3. Contact time effect

Figure 7 shows the variation in the amount of MB adsorbed as a function of contact time. The results obtained allow us to conclude that the adsorption rate of MB was rapid during the first 40 minutes of contact between the solution and the adsorbent, which is explained by the large number of active sites available on the surface of the adsorbent, thus promoting significant removal activity [33]. Beyond this time, the process slowed down, reaching equilibrium at 80 minutes. The equilibrium adsorption capacity of MB is 37.64 mg/g, indicating saturation of most of the active sites on the adsorbent.

Kinetic models were necessary to study adsorption properties, examine equilibrium parameters, and understand the nature of interactions between the adsorbate and the adsorbent [34]. The kinetic data relating to the adsorption of BM on pyrophyllite were analysed using two kinetic models, namely the pseudo-first-order (PFO) model and the pseudo-second order (PSO) model.

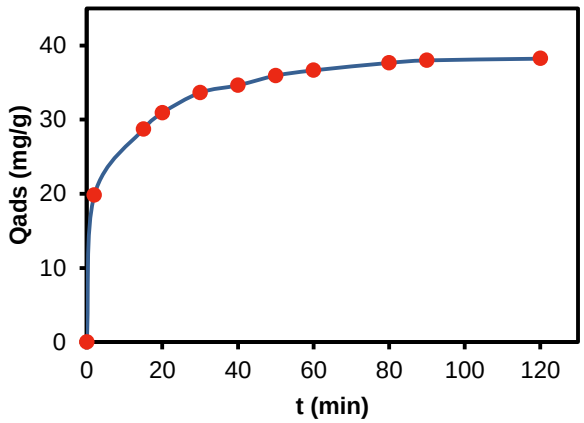

Fig. 7. Influence of contact time on the adsorption of BM by pyrophyllite clay (pH = 6,84, C_0 = 20 ppm, R = 0,5 g/L, T = 25 °C)

Table 2 summarises the kinetic parameters calculated from the graphical representation of these two models, as well as the correlation coefficient (R^2) value for each model. The correlation coefficient found for the pseudo-second-order kinetics (R^2 = 0.9968) was higher than that for the pseudo-first-order kinetics (R^2 = 0.9794). By comparing the adsorption capacity calculated by the pseudo-second-order model with the experimental value, it is clear that this model is the most appropriate for describing the adsorption phenomenon.

3.2.4. Initial dye concentration effect

Different initial concentrations of BM dye were studied: 5, 10, 20, 48.3, 76.75, 93.18 and 128 ppm. The solid/liquid ratio used was 0.5 g/l, with a contact time of 80 minutes at a temperature of 25 °C, pH = 6.84. The influence of the initial concentration on the amount of MB adsorbed by pyrophyllite is shown in Figure 8. According to the results obtained, the amount of MB adsorbed increases with the initial concentration until it reaches a state of equilibrium. This can be attributed to the increase in the transfer of the adsorbate from the aqueous solution to the surface of the adsorbent (under the effect of the driving force of concentration) until the active sites of the clay are saturated at high dye concentrations [35].

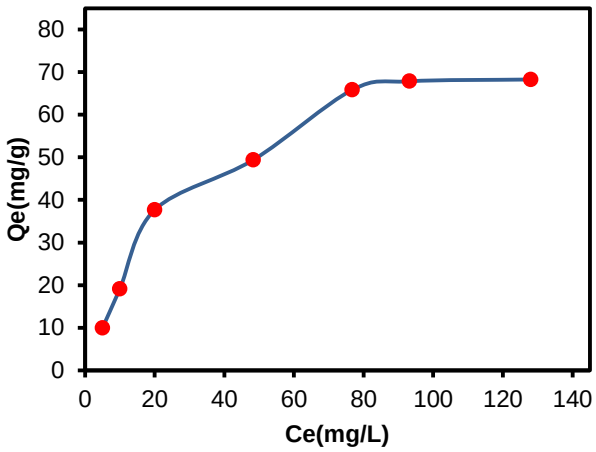

Fig. 8. Effect of initial concentration on BM adsorption on pyrophyllite

3.2.5. Temperature effect

The temperature effect (Figure 9) illustrates how temperature variation affects MB adsorption on clay. We used the same ratio and initial MB concentration as indicated above. The adsorption study was carried out at the following temperatures: 25, 35, 45 and 55 °C, with a contact time of 80 min, mass, C_i and pH. The results clearly show that as the temperature increases, the adsorption capacity increases, demonstrating the positive effect of temperature increase on pyrophyllite. This increase in temperature facilitates the diffusion of adsorbed molecules into the internal pores of the adsorbing particles by reducing the viscosity of the solution [36].

Table 2.
Kinetic parameters of MB adsorption on pyrophyllite

$Q_{e.exp}$ (mg.g^{-1})	Pseudo First-order			Pseudo second-order		
37,64	$Q_{e.1}$ (mg.g^{-1})	K_1 (min^{-1})	R^2	$Q_{e.2}$ (mg.g^{-1})	K_2 (g.mg^{-1}.min^{-1})	R^2
	23,06	0,0485	0,9794	39,21	0,00611	0,9968

Table 3.
Thermodynamic parameters of MB dye adsorption on pyrophyllite

ΔH° (kJ.mol^{-1})	**ΔS°** (J.mol^{-1}.K^{-1})	**ΔG°**(kJ.mol^{-1})			
		298K	***308K***	***318K***	***328K***
53,52	208,79	- 8,69	- 10,78	- 12,87	- 14,96

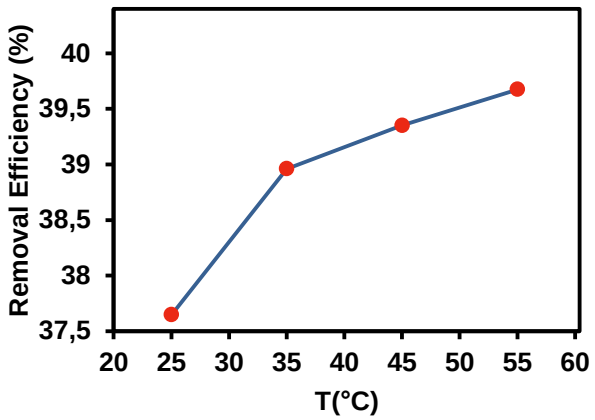

Fig. 9. Temperature effect on MB adsorption by pyrophyllite

In order to better understand the mechanisms governing adsorption and explain the thermodynamic behaviour of the process, this study was based on the evaluation of the following thermodynamic parameters: entropy change (ΔS°), enthalpy change (ΔH°) and Gibbs free energy (ΔG°). The results were interpreted using equations (Eq.3-5).

$$ln(k_d) = \frac{\Delta S^\circ}{R} - \frac{\Delta H^\circ}{RT} \qquad (Eq.3)$$

$$k_d = \frac{Q_e}{C_e} \qquad (Eq.4)$$

$$\Delta G^\circ = \Delta H^\circ - \Delta S^\circ \qquad (Eq.\ 5)$$

Where R is the ideal gas constant (8.314 J.mol^{-1}.K^{-1}); T is the temperature (in kelvins, K); K_d is the equilibrium constant.

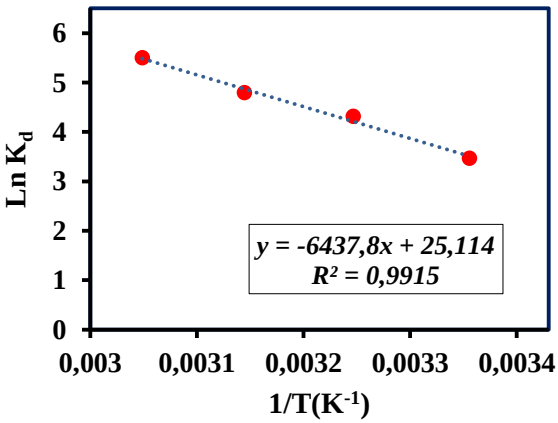

Fig. 10. Variations in Ln Kd as a function of 1/T for BM adsorption on pyrophyllite

The thermodynamic factors (ΔG°, ΔH°, and ΔS°) obtained from the y-intercept and slope of the curve (Ln K_d) as a function of 1/T (Figure 10) are shown in Table 6. The ΔG° evaluated at all temperatures was negative, which means that the MB adsorption process on clay is spontaneous. The ΔS° value obtained is positive, indicating an increase in disorder at the solid-liquid interface. The ΔH° obtained is also positive, indicating an endothermic adsorption process [37]. Furthermore, the amplitude of ΔH° allows the type of sorption to be estimated (Table 3). During physical adsorption, the heat released (between 2.1 and 20.9 kJ/mol) is comparable to the heat of condensation, while the heat of chemisorption is generally between 80 and 200 kJ/mol. The ΔH° value of 53.52 kJ/mol, determined for MB adsorption on pyrophyllite in this study, suggests a combined mechanism involving both physical and chemical interactions.

3.3. Adsorption isotherm

The adsorption isotherm explains how the adsorbate molecules position themselves between the liquid phase and the solid phase when the adsorption process reaches a state of equilibrium [38]. The experimental data obtained on the adsorption equilibrium of BM on pyrophyllite were modelled using two models, the Langmuir model and the Freundlich model. Figures 11 and 12 show the fitting curves for the Langmuir and Freundlich models. Table 4 presents the constants of the MB adsorption isotherms on pyrophyllite. The Langmuir model gives a maximum adsorption capacity Qm = 69.44 mg/g and an excellent fit (R^2 = 0.9922), indicating single-layer adsorption on a homogeneous surface. The Freundlich model also shows favourable adsorption (1/n = 0.2392, K_F = 25.43), but with a slightly poorer fit (R^2 = 0.9493). It appears that the Langmuir model has the highest correlation coefficient (0.9922) compared to the Freundlich model (0.9493), indicating that it is the most suitable model for describing adsorption equilibrium. The value of Langmuir's separation factor K_L is between 0 and 1. This suggests that the Langmuir isotherm is favourable for the adsorption of MB on pyrophyllite clay. The adsorption of MB dye was dominant in the monolayer mode on the homogeneous surface of the adsorbent with no interactions between the retained molecules.

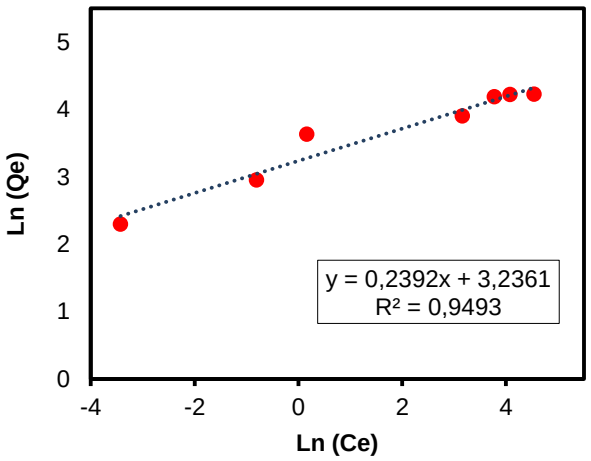

Fig. 11. Langmuir linear form of MB adsorption on pyrophyllite

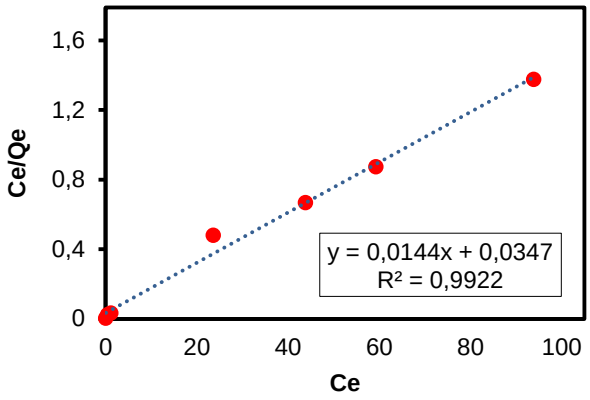

Fig. 12. Freundlich linear form of MB adsorption on pyrophyllite

Table 4
Constants of MB adsorption isotherms on pyrophyllite

Modèle de Langmuir			Modèle de Freundlich		
Q_m (mg/g)	k_L	R^2	1/n	K_F	R^2
69,44	0,41	0,9922	0,2392	25,43	0,9493

4. Conclusion

In the present study, raw pyrophyllite clay, an abundant and low-cost material, was employed as an adsorbent to evaluate its capacity for removing methylene blue (MB) from aqueous solutions. Its surface properties and structure were thoroughly characterized by X-ray diffraction (XRD), scanning electron microscopy (SEM), and Fourier-transform infrared spectroscopy (FTIR).

A series of batch adsorption experiments was conducted to assess the influence of key operational parameters, including adsorbent dosage, initial dye concentration, contact time, temperature, and pH, in order to determine the optimal conditions for MB removal. The results showed that the maximum removal efficiency was achieved using 10 mg of adsorbent, a contact time of 80 min, and a pH of 6. The adsorption yield increased with the adsorbent mass-to-solution volume ratio. Kinetic data were best fitted by the pseudo-second-order model, while the Langmuir isotherm provided the most suitable description of the equilibrium data. The calculated thermodynamic parameters (ΔS°, ΔG°, and ΔH°) indicated a favorable, spontaneous, and endothermic adsorption process. An increase in MB removal efficiency was observed over the entire pH range studied, suggesting that, under the investigated conditions, pH has a limited influence on pyrophyllite adsorption performance.

Overall, these findings demonstrate the effectiveness of the selected raw pyrophyllite clay for the removal of methylene blue from aqueous solutions. Future work should focus on exploring the regeneration and reusability of this material. Given its promising performance, this raw clay warrants further evaluation for the treatment of industrial wastewater containing various pollutants, and the development of modified pyrophyllite-based materials to enhance adsorption efficiency.

Bibliographic references

[1] I. Khan, K. Saeed, I. Zekker, B. Zhang, A. H. Hendi, A. Ahmad, S. Ahmad, N. Zada, H. Ahmad, L. A. Shah, et al. Review on Methylene Blue: Its Properties, Uses, Toxicity and Photodegradation. Water. (2022).
[2] E. Fayad, M. Alsunbul, R. S. Alazragi, A. Ebada, H. S. Ali, M. F. Mubarak. Magnetic chitosan kaolinite cellulose nanofibril cryogel beads for efficient removal of methylene blue from water. (2025) 1–26.
[3] K. Allam, K. Gourai, B. Belhorma, L. Bih. Adsorption of Methylene Blue on raw and activated Clay: case study of Bengurir clay. 2508(6) (2018) 1750–1761.
[4] M. Chahal, S. Kumari, A. Bhattacharya, M. C. Garg. Evaluating sustainable agricultural waste biomass for methylene blue adsorption in wastewater treatment: A state-of-the-art review. Bioresour. Technol. Rep. 28 (2024) 101983.
[5] H. Jadeppa, P. S. Kumar, B. P. Ravi. Process characterization of a low-grade pyrophyllite from Nambulapulakunta, Anantapur, Andhra Pradesh. 26(3) (2024) 2024.
[6] M. A. Ali, H. A. M. Ahmed, H. M. Ahmed. Pyrophyllite: An Economic Mineral for Different Industrial Applications. Appl. Sci. (2021).
[7] B. Biswas, R. Islam, A. K. Deb, A. Greenaway, L. N. Warr, R. Naidu. Understanding Iron Impurities in Australian Kaolin and Their Effect on Acid and Heat Activation Processes of Clay. ACS Omega. (2023).
[8] M. Lamrani, M. Mouchane, H. Taybi, A. Mouadili. Comprehensive Review on the Adsorption Properties of Clay Minerals for Enhanced Removal of Toxic Dyes and Heavy Metals. J. Water Environ. Nanotechnol. 10(1) (2025) 85–107.
[9] A. El Azizi, S. Maliki, K. Hamidallah, A. Chahid, H. El Harouachi, A. Zourif, M. Mansori, M. Loutou. Eco-friendly natural Moroccan clay as a high-performance adsorbent for methylene blue removal: integrated experimental characterization and computational modeling. Environ. Sci. Pollut. Res. 32(26) (2025) 15695–15715.
[10] E. M. Saad, M. Wagdy, A. S. Orabi. Advanced nano modification of ecofriendly glauconite clay for high efficiency methylene blue dye adsorption. Sci. Rep. (2024) 1–20.
[11] Y. Ettahiri, L. Bouna, J. V. Hanna, A. Benlhachemi, H. L. Pilsworth, A. Bouddouch, B. Bakiz. Pyrophyllite clay-derived porous geopolymers for removal of methylene blue from aqueous solutions. Mater. Chem. Phys. 296 (2023) 127281.
[12] A. M. Elgarahy. A comprehensive review on sustainable clay-based and future outlook Compounds. Springer International Publishing. (2023).

[13] A. El, Y. Miyah, L. Nahali, F. Zerrouq, B. El. Fast adsorption for removal of methylene blue from aqueuous solutions using of local. 3 (2019) 416–423.
[14] I. Dawood, A. H. Zyoud, S. Zyoud, A. Amireh, S. H. Zyoud, T. W. Kim. Sustainable water treatment using thermally stable natural clay: dual adsorption – thermolysis approach for organic pollutants and nitrate removal. (2025) 1–13.
[15] A. Hsini, A. Essekri, N. Aarab, M. Laabd, A. Ait Addi, R. Lakhmiri, A. Albourine. Elaboration of novel polyaniline@Almond shell biocomposite for effective removal of hexavalent chromium ions and Orange G dye from aqueous solutions. Environ. Sci. Pollut. Res. 27(13) (2020) 15245–15258.
[16] M. Atif, H. Zeshan, R. Bongiovanni, M. Fayyaz, T. Razzaq, S. Gul. Physisorption and chemisorption trends in surface modification of carbon black. Surf. Interfaces. 31 (2022) 102080.
[17] S. Wang, L. Gainey, I. D. R. Mackinnon, C. Allen, Y. Gu, Y. Xi. Thermal behaviors of clay minerals as key components and additives for fired brick properties: A review. J. Build. Eng. 66 (2023) 105802.
[18] J. T. Kloprogge. Raman Spectroscopy of Clay Minerals. In: W. P. Gates, J. T. Kloprogge, J. Madejová, F. Bergaya (Eds.), Infrared and Raman Spectroscopies of Clay Minerals. Vol. 8. Elsevier. (2017) 150–199.
[19] F. Largo, R. Haounati, S. Akhouairi, H. Ouachtak, R. El, A. Jada, A. Ait. Adsorptive removal of both cationic and anionic dyes by using sepiolite clay mineral as adsorbent: Experimental and molecular dynamic simulation studies. J. Mol. Liq. 318 (2020).
[20] B. Ennasraoui, H. Ighnih, R. Haounati, M. Rhaya, R. E. Malekshah, S. Alahiane, H. Ouachtak, A. Jada, A. Ait Addi. Enhanced solar-driven photocatalytic decomposition of ciprofloxacin antibiotic and Orange G dye using innovative g-C3N4/BiOCl/Ag2MoO4 nanocomposites: Experimental and Monte Carlo simulation studies. J. Mol. Liq. 429 (2025) 127476.
[21] R. Haounati, E. Amaterz, A. A. Addi. Experimental and molecular dynamics simulation study on the adsorption of Rhodamine B dye on magnetic montmorillonite composite γ-Fe2O3@Mt. J. Mol. Liq. (2020) 113142.
[22] H. Ighnih, R. Haounati, H. Ouachtak, A. Regti, B. El Ibrahimi, N. Hafid, A. Jada, M. Labd Taha, A. A. Addi. Efficient removal of hazardous dye from aqueous solutions using magnetic kaolinite nanocomposite: Experimental and Monte Carlo simulation studies. Inorg. Chem. Commun. 153 (2023) 110886.
[23] M. A. Ali, H. A. M. Ahmed. Chemical and Mineralogical Characterization of Saudi-Pyrophyllite ore and its potential applications. 39(1) (2022) 1–18.
[24] Y. Miyah, A. Lahrichi, M. Idrissi. Assessment of adsorption kinetics for removal potential of Crystal Violet dye from aqueous solutions using Moroccan pyrophyllite. J. Assoc. Arab Univ. Basic Appl. Sci. (2017) 20–28.
[25] A. Talidi, A. Bouazizi, A. Essate, A. Karim. Manufacture and characterization of flat microfiltration membrane based on Moroccan pyrophyllite clay for pretreatment of raw seawater for desalination. Desalin. Water Treat. 253 (2022) 24–38.
[26] S. K. Jena, N. Dhawan, D. S. Rao, P. K. Misra, B. Das. Extraction of potash values from pyrophyllite mine waste. Sep. Sci. Technol. 51(2) (2016) 269–277.
[27] Y. Miyah, A. Lahrichi, R. Kachkoul, G. El Mouhri, M. Idrissi, S. Iaich, F. Zerrouq. Multi-parametric filtration effect of the dyes mixture removal with the low cost materials. Arab J. Basic Appl. Sci. 27(1) (2020) 248–258.
[28] M. O. Yusuf. Bond Characterization in Cementitious Material Binders Using Fourier-Transform Infrared Spectroscopy. Appl. Sci. (2023).
[29] S. Adlane, A. Essate, J. Naim, B. Achiou, A. Tiraferri, A. Aaddane, S. Youssefi, M. Ouammou, S. Alami. Development and characterization of a purified pyrophyllite-based ultrafiltration membrane for the treatment of dye-contaminated water. J. Environ. Chem. Eng. 13(5) (2025) 118579.
[30] G. Sarojini, S. Venkateshbabu, M. Rajasimman. Facile synthesis and characterization of polypyrrole - iron oxide e seaweed (PPy-Fe3O4-SW) nanocomposite and its exploration for adsorptive removal of Pb(II) from heavy metal bearing water. Chemosphere. 278 (2021) 130400.
[31] R. Liu, B. Zhang, D. Mei, H. Zhang, J. Liu. Adsorption of methyl violet from aqueous solution by halloysite nanotubes. Desalination. 268(1–3) (2011) 111–116.
[32] G. A. El, A. I. Abd-elhamid, O. O. M. Farahat, A. A. El-bardan, H. M. A. Soliman, A. A. Nayl. Adsorption of crystal violet and methylene blue dyes using a cellulose-based adsorbent from sugercane bagasse: characterization, kinetic and isotherm studies. J. Mater. Res. Technol. 19 (2022) 3241–3254.
[33] R. Sahraei, K. Hemmati, M. Ghaemy. Adsorptive removal of toxic metals and cationic dyes by magnetic adsorbent based on functionalized graphene oxide from water. RSC Adv. 6(76) (2016) 72487–72499.
[34] H. Saadani, H. Abara, S. Akachar, J. Raissouni, M. Hadri, K. Draoui. Enhanced Removal of Nickel from Aqueous Solutions Using Carbonated Moroccan Clay: Characterization, Adsorption and Thermodynamic Studies. 13(3) (2025) 993–1011.
[35] A. Imgharn, M. Laabd, Y. Naciri, A. Hsini. Insights into the performance and mechanism of PANI @ Hydroxapatite-Montmorillonite for hexavalent chromium Cr(VI) detoxification. Surf. Interfaces. 36 (2023) 102568.
[36] E. Fosso-kankeu, H. Mittal, F. Waanders, S. Sinha. Thermodynamic properties and adsorption behaviour of hydrogel nanocomposites for cadmium removal from mine effluents. J. Ind. Eng. Chem. 48 (2017) 151–161.
[37] H. S. Shin, J. Kim. Isotherm, kinetic and thermodynamic characteristics of adsorption of paclitaxel onto Diaion HP-20. Process Biochem. 51(7) (2016) 917–924.
[38] Y. Abdellaoui, H. Abou, A. Hsini, B. El. Synthesis of zirconium-modified Merlinoite from fly ash for enhanced removal of phosphate in aqueous medium: Experimental studies supported by Monte Carlo / SA simulations. Chem. Eng. J. 404 (2021) 126600.